PRAMANA
— journal of
physics

Vol. 55, No. 3
September 2000
pp. 455–469

Annealing effect on transport properties of $Nd_{0.67}Sr_{0.33}MnO_3$ thin films

M PATTABIRAMAN[a], P MURUGARAJ[a], G RANGARAJAN[a], V PRASAD[b], S V SUBRAMANYAM[b], V S SASTRY[c], SANG-MO KOO[d] and K V RAO[d]

[a]Department of Physics, Indian Institute of Technology, Chennai 600 036, India
[b]Department of Physics, Indian Institute of Science, Bangalore 560 012, India
[c]Materials Science Division, Indira Gandhi Centre for Atomic Research, Kalpakkam, 603 102, India
[d]Department of Physics, Royal Institute of Technology, SE-100 44 Stockholm, Sweden

MS received 4 March 2000; revised 23 August 2000

Abstract. Annealing dependence of the lattice parameter, resistivity, magnetoresistance and thermopower have been studied on $Nd_{0.67}Sr_{0.33}MnO_3$ thin films deposited on $LaAlO_3$ and alumina substrates by pulsed laser ablation. Upon annealing at 800°C and 1000°C the lattice constant of the $LaAlO_3$ film tends toward that of the bulk target due to reduction in oxygen vacancies. This results in a metal–insulator transition at temperatures which increase with progressive annealing along with a decrease in the observed low temperature MR. Using a magnon scattering model we estimate the e_g bandwidth of the film annealed at 1000°C and show that the magnon contribution to the resistivity is suppressed in a highly oxygen deficient film and gains prominence only upon subsequent annealing. We also show that upon annealing, the polaron concentration and the spin cluster size increases in the paramagnetic phase, using an adiabatic polaron hopping model which takes into account an exchange dependent activation energy above the resistivity peak.

Keywords. Colossal magnetoresistance; polaron; metal–insulator transition; thermopower; oxygen deficiency; manganite.

PACS Nos 75.30.Vn; 71.38.+i; 71.30.+h

1. Introduction

Since the discovery of colossal magnetoresistance in alkaline earth doped rare earth manganites of the general formula $R_{1-x}A_x\mathrm{MnO_3}$ ($R = \mathrm{Nd, La}; A = \mathrm{Ca, Sr}$) there has been an intense effort to fabricate and characterize thin films which could be used as magnetosensitive devices [1]. However this has proved difficult to achieve because the observed magnetotransport properties in epitaxial films are very sensitive to the strain induced by the film-substrate lattice mismatch [2] and oxygen deficiency [3]. While the former effect is prominently observed in thin films (∼1000 Å) the latter is seen in both thin and thick films (∼5000 Å) [4]. The CMR properties of these films are dependent crucially on the oxygen stoichiometry and they need to be annealed after deposition. Well characterized experimental data as a function of strain and oxygen deficiency is necessary for comparing the

various results published in the literature and for the use of these materials as commercial magnetosensitive devices. Many groups have studied the effect of misfit stress on the magnetoresistive properties [4,5]. In this report we progressively remove the oxygen deficiency in an as-prepared $Nd_{0.67}Sr_{0.33}MnO_3$ (NSMO) thin film pulsed laser deposited (PLD) on $LaAlO_3$, by annealing in air and monitor the changes in lattice parameter, resistivity, magnetoresistance and thermopower. $LaAlO_3$ was chosen as the substrate to study the role of oxygen deficiencies because among the popular PLD substrates like MgO and $SrTiO_3$, $LaAlO_3$ films exhibit good epitaxy and have relatively fewer dislocations [4]. We have also studied material of the same composition deposited on amorphous alumina, which has been used as a substrate for the MOCVD growth of manganites [6]. The oxygen deficiency induced disorder is evaluated using a magnon scattering model below $\sim 0.5T_{\rm P}$ ($T_{\rm P}$ is the temperature at which a peak is observed in the resistivity) and an adiabatic polaron hopping model which takes into account an exchange dependent activation energy above $T_{\rm P}$.

2. Experiment

Polycrystalline sintered ceramic discs of NSMO prepared by conventional solid state reaction were used as targets in a PLD unit using a NY81-C Nd:YAG laser and a custom-made Neocera deposition chamber on $LaAlO_3$ (001) and amorphous Al_2O_3 substrates at 800°C in 300 m Torr O_2 atmosphere. The wavelength, pulse frequency and focussed energy density of the beam were 355 nm, 10 Hz, $\sim$3 J/cm^2 respectively and the target–substrate distance was 50 mm. The thickness of the film is estimated to be about 4000 Å from the deposition time of 20 min. X-ray measurements were performed on a STOE diffractometer. Thermopower measurements were made on a home-made apparatus and magnetoresistance measurements were performed using a JANIS 'supervaritemp' cryostat in applied fields of up to 6.4 T, at temperatures down to 4.2 K.

3. Results and discussion

3.1 *X-ray diffraction*

The XRD pattern (figure 1a) of the NSMO film on $LaAlO_3$ (N1) showed good c-axis orientation (only (00l) peaks present) with a lattice constant (a_0) of 3.882 Å ($a_0 = 3.773$ Å for $LaAlO_3$) while a_0 for the bulk target is 3.857 Å. Upon annealing at 800°C for 5 hours in air, the lattice constant decreased to 3.875 Å (figure 1b). Subsequent annealing at 1000°C for 5 hours in air resulted in a further decrease to 3.863 Å. Thus upon progressive annealing a_0 tends towards the bulk value. This decrease is due to the removal of oxygen vacancies. Annealing also removes strain but this should be insignificant in the relatively thick film used in this study.

The XRD pattern of the NSMO film on amorphous alumina (N2) (figure 1c) also showed predominant c-axis orientation but with an additional peak in the (011) direction with $a_0 =$ 3.865 Å. Upon annealing at 800°C for 5 hours in air a_0 decreased to 3.855 Å indicating a reduction in lattice defect concentration.

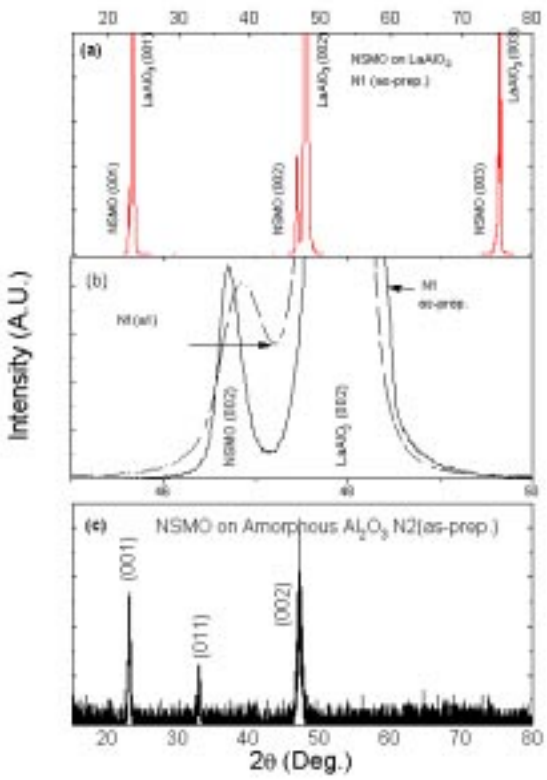

Figure 1. X-ray diffractograms for films N1 and N2.

3.2 *Resistivity*

The 'as-prepared' films N1 and N2 were semiconducting with no insulator–metal (IM) transition (figure 2a). Annealing at 800°C resulted in a drastic reduction in resistivity ($\rho_{300\ \mathrm{K}} = 1.95\ \Omega$m for as-prepared N1 and $0.71 \times 10^{-3}\ \Omega$m after the first annealing) and an IM transition was observed at 165 K (figure 2b). Upon further annealing at 1000°C, $\rho_{300\ \mathrm{K}}$ decreased further ($\rho_{300\ \mathrm{K}} = 0.13 \times 10^{-3}\ \Omega$m after the second annealing) and a sharper IM transition was seen at 194 K (figure 2b).

In the manganites the hopping probability of the e_g electron from Mn^{3+} to the Mn^{4+} ion depends on the Mn–O–Mn bond angle [2]. In highly oxygen deficient films, broken Mn–O–Mn bonds inhibit charge transport and the onset of ferromagnetism. This results in pure semiconducting behaviour. Annealing leads to a replenishment of the oxygen sublattice and enhances the hopping probability of the mobile e_g electron resulting in ferromagnetism accompanied by an insulator–metal transition.

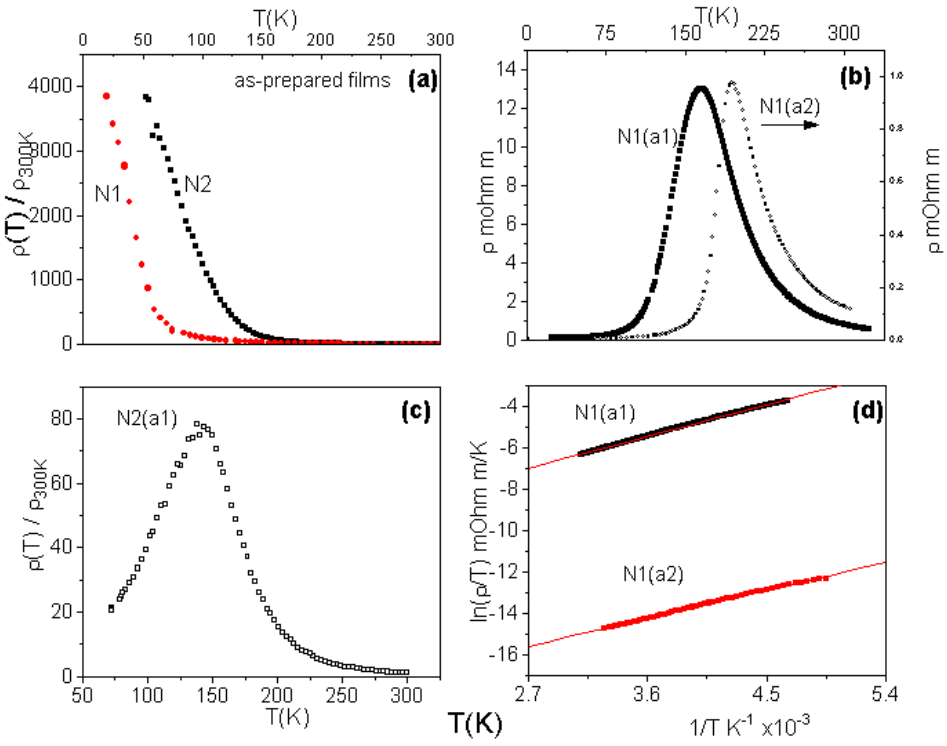

Figure 2. (**a**) $\rho(T)$ for as-prepared N1 and N2, (**b**) $\rho(T)$ for N1a1 and N1a2, (**c**) $\rho(T)$ for N2a1, (**d**) fit to adiabatic polaron hopping model (eq. (1a)) for N1a1 and N1a2.

Table 1. Lattice constants for N1 and N2 as a function of annealing.

Film status	N1 (a_0) Å	N2 (a_0) Å
As-prepared (bulk $a_0 = 3.857$ Å)	3.882	3.865
800°C annealed in air (5 hours)	3.875	3.855
1000°C annealed in air (5 hours)	3.863	3.841

After annealing at 800°C, a broad IM transition was seen at 133 K for N2 (figure 2c). Upon annealing this film at 1000°C the IM transition was no longer seen and the film was semiconducting. To understand this effect we tabulate the observed lattice constants in table 1. While the decrease in a_0 seen in N1 can be attributed to a decrease in the number of defects, the same cannot be said about N2a2 since the film turned semiconducting. Two things could have happened when N2 was annealed at 1000°C: (a) Oxygen could have left the lattice and (b) Al from the substrate could have replaced some of the Mn ions in the

film resulting from reaction with the substrate material. The first possibility can be ruled out because O_2 deficient samples have a larger a_0 than O_2 richer samples [7]. Since Al is a smaller ion than Mn, its replacement would lead to a decrease in a_0. This would account for the trend observed and is a limitation of using amorphous alumina films. A similar trend has been observed in studies of solid oxide fuel cells where Al doping of the Mn site in LSMO had resulted in a large increase in resistivity [8].

3.2.1 *High temperature resistivity*: High temperature resistivity measurements establish the high temperature transport to be due to magnetic polaron hopping [9]. In order to study the effect of annealing on polaronic transport, the $\rho(T)$ data was fitted to both the adiabatic as well as non-adiabatic polaron hopping models of Emin and Holstein [10] (figure 2d).

Adiabatic polaron hopping: In this case the relevant optical mode lattice fluctuation is long lived compared to the electron tunnelling event and the hopping rate is given by the expression $W = 2\pi\nu \exp(-E_{\rm A}/kT)$ [10]

$$\rho = BT \exp\left[\frac{E_{\rm A}}{k_{\rm B}T}\right], \tag{1a}$$

with $B = ah/(e^2c(1-c)T_0)$.

Non-adiabatic polaron hopping: In the non-adiabatic limit the electron tunneling event is not necessarily fast compared to the relevant optical-mode lattice fluctuation. The hopping rate then carries a temperature-dependent prefactor

$$W = J^2\pi^{1/2} \exp(-E_{\rm A}/kT)/[4E_{\rm A}k_{\rm B}T]^{1/2},$$

where the electron transfer matrix element J is assumed to be much smaller than the lattice relaxation energy.

$$\rho = B'T^{1.5} \exp\left[\frac{E_{\rm A}}{k_{\rm B}T}\right], \tag{1b}$$

with $B' = ah/(e^2c(1-c)T_0^{1.5})$, where a is the site to site hopping distance, c the polaron concentration and T_0, a temperature characteristic of the longitudinal optical phonon frequency. Using the values of c obtained from thermopower measurements (see below), we can determine the longitudinal optical phonon frequency (ν) (table 2).

Table 2. Fit parameters to adiabatic polaron hopping. The values within parenthesis correspond to the non-adiabatic case.

Sample	B $\Omega\,\mathrm{mK}^{-1}$ $\times 10^{-9}$	T_0 K	$\nu_{\rm cal}$ $\mathrm{s}^{-1}\times 10^{-14}$	$E_{\rm A}$ meV	E_S meV	W_H^* meV
N1a1	9.4 (32.2)	5313 (2733)	1.1 (5.7)	146.5 (159.8)	12.2	134.3 (147.6)
N1a2	2.8 (9.8)	16100 (6039)	3.4 (12.5)	129.7 (143.2)	11.4	118.3 (131.8)

$^*W_H = E_{\rm A} - E_S + J \approx E_{\rm A} - E_S$; $W_H >> J$ (the criterion for polaron formation), where J is the transfer integral and W_H is one half of the polaron formation energy.

The values of $\nu_{\rm cal}$ are comparable to those obtained from transport data [2]. The criterion for non-adiabatic behaviour is that the calculated T_0 ($\nu_{\rm cal}$) should be much less than the experimental longitudinal optical phonon frequencies ($\nu_{\rm ex}$) [10]. $\nu_{\rm ex}$ values obtained from the phonon peaks in the optical conductivity data for $La_{0.825}Sr_{0.175}MnO_3$ range from $10^{12-13}s^{-1}$ [11] and are comparable to the estimated values. Thus since these materials lie close to the region separating adiabatic and non-adiabatic behaviour it is difficult to discriminate between the two models as noted before [12].

An activation energy ($E_{\rm A}$) of 146.5 meV was obtained for N1a1 (800°C annealing), 160.3 meV for N2a1 and 129.7 meV for N1a2 (1000°C annealing). These are much higher than those obtained for well annealed LCMO ($x = 0.33$) DC sputtered films [13] (80–117 meV for three different samples of the same composition) which again points to the high oxygen deficiency in these samples. If we assume the polaron to be trapped in a potential well of height $E_{\rm A}$, an oxygen deficient lattice is heavily distorted and the polaron would have to surmount a higher energy barrier to free itself. The 1000°C anneal results in partial replenishment of the oxygen sublattice resulting in a large decrease in $E_{\rm A}$.

3.2.2 *Low temperature resistivity*: Different equations have been used to characterize the low temperature resistivity of the manganites. LCMO polycrystalline pellets and film have been found to obey the equation: $\rho = \rho_0 + \rho_1 T^{2.5}$ [14, 15]. Urshibara *et al* [16] obtained a T^2 dependence for LSMO which was interpreted as being due to electron–electron scattering. Kubo and Ohata [17] predicted a $T^{4.5}$ dependence for the resistivity at low temperatures for a double exchange ferromagnet. The $T^{4.5}$ dependence has been observed in manganites but along with a T^2 contribution at lower temperatures [18]. Recently Jaime *et al* [19] and Broussard *et al* [20] have used the following form:

$$\rho = \rho_0 + \rho_2 T^2 + \rho_5 T^5. \tag{2}$$

Both groups observe a deviation from the T^2 dependence at low temperatures (below $0.2T_{\rm C}$). Jaime *et al* [19] have interpreted this as due to the collapse of the minority sub-band as each local down-spin hole aligns parallel to the spin core. Thus $\rho_2 T^2$ represents single magnon scattering and $\rho_5 T^5$ the contribution from electron–phonon processes. Table 3 lists the parameters obtained for N1a1, N1a1 at $6.4T$ and N1a2.

We find that none of the above relations are obeyed in the case of the oxygen deficient film N1a1. The data is found to fit best to an exponent of 4 rather than 5 at low temperatures without a T^2 dependence ($\rho = \rho_0 + \rho_4 T^4$) (figure 3). Below 20 K there is a sharp upturn in the resistivity (figure 4a). This behaviour has recently been ascribed to strong electron–electron interactions (akin to a disordered metal) [21]. However since it has not been observed in single crystals [19] it is more likely due to the oxygen deficiency. Moreover the resistivity upturn is strongly suppressed when a $6.4T$ magnetic field is applied (figure 4b). The oxygen deficiency induces an inhomogenous magnetization, which is partially removed by the field. Thus an applied field enhances spin polarization and therefore the electron mobility suppresses disorder scattering resulting in a large magnetoresistance.

After annealing at 1000°C there is a drastic reduction in $\rho_0 (\rho_0 \ll \rho_0'')$ and N1a2 exhibits a T^2 and a T^5 dependence (figure 5a, b). However the value of ρ_2 obtained as the slope in the ρ vs T^2 fit is not equal to the ρ_2 obtained as an intercept in the $(\rho - \rho_0)/T^2$ vs T^3 plot as the temperature range of the two fits overlap. Thus there is no clear separation between the

Table 3. Low temperature resistivity fitting parameters.

Sample	T^2 fit ρ vs T^2		T^5 fit $(\rho-\rho_0)/T^2$ vs T^3			T^4 fit	
	$\rho_0^{\dagger}$ 10^{-5} Ωm	ρ_2 $\times 10^{-10}$ ΩmK^{-2}	ρ_2 intercept $\times 10^{-10}$ ΩmK^{-2}		ρ_5 $\times 10^{-17}$ ΩmK^{-5}	ρ_0'' 10^{-5} Ωm	ρ_4 $\times 10^{-14}$ ΩmK^{-4}
N1a1	–	–	–		–	11.8 (20–75 K)	669.3
N1a2	0.4 (20–73 K)	3.9	1.3 (79–133 K)	45.2	48.6* (63–133 K)	–	–
$La_{0.67}(Ca_xSr_{1-x})_{0.33}MnO_3$ films [20]	0.15 $(x=1)$	1.2	–		~ 1	–	–
N1a1 $H = 6.4T$	–	–	–	–	641.7‡ (72–159 K)	5.3 (58–115 K)	74.3

† Since these films exhibit a small upturn in the resistivity at low temperatures $(T < 0.1T_C)$ ρ_0 should be treated as an intercept and not as residual resistivity.
* This value was obtained from a plot of ρ vs T^5. An intercept of 0.5×10^{-5} Ωm was obtained.
‡ Obtained from a plot of ρ vs T^5 (72–159 K) with an intercept of 6.2×10^{-5} Ωm.

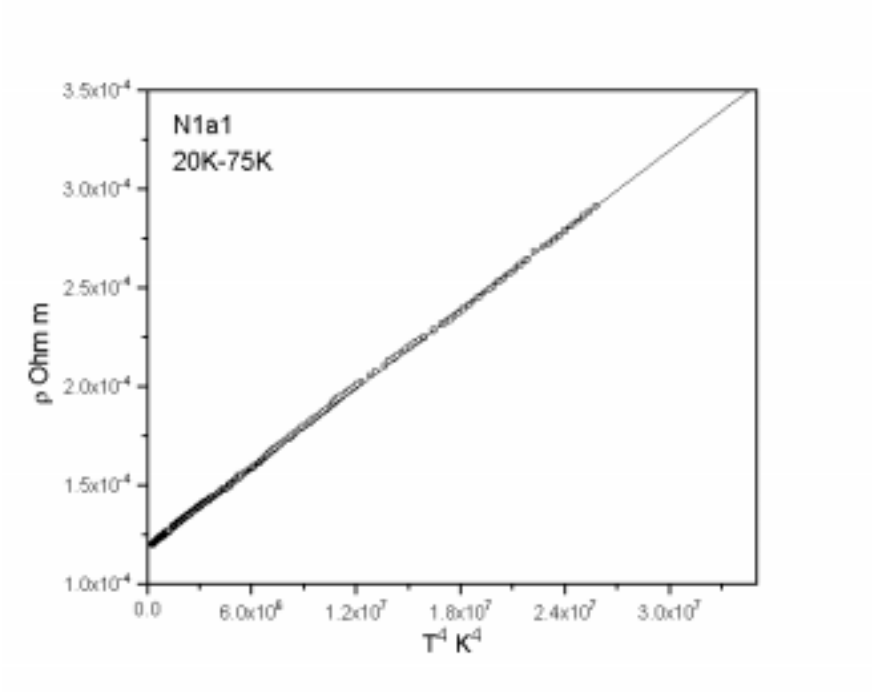

Figure 3. The low temperature T^4 dependence of $\rho(T)$ seen in N1a1.

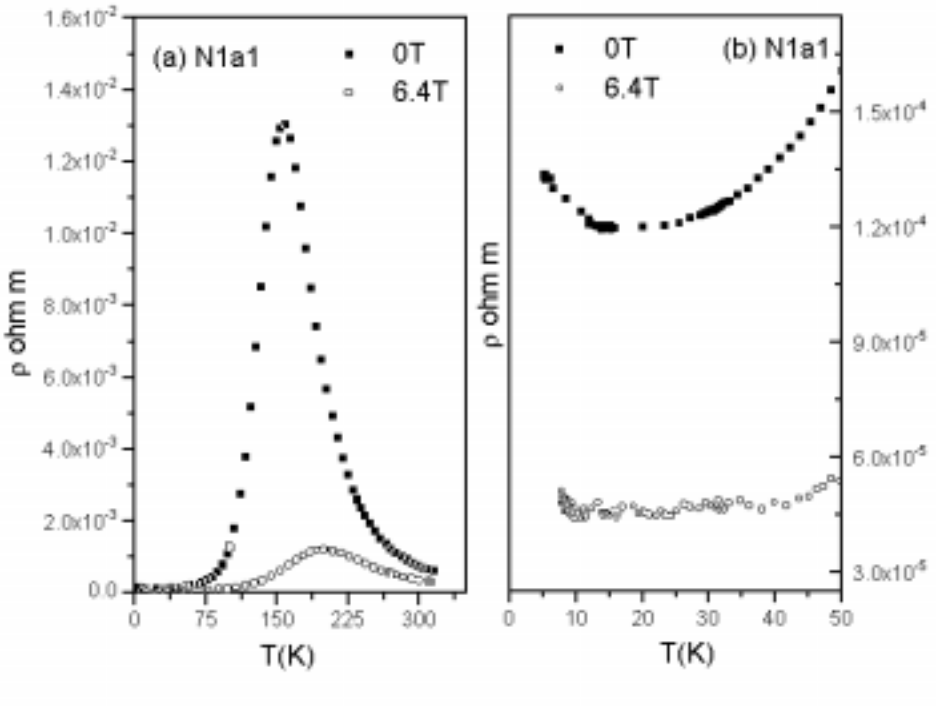

Figure 4. (**a**) $\rho(T)$ at $0T$ and $6.4T$ for N1a1, (**b**) the low temperature resistivity upturn in N1a1 and its suppression on application of a $6.4T$ field.

T^2 and T^5 regions and the data for N1a2 can be fitted to a form $\rho = \rho_0 + \rho_5 T^5$ (figure 5c) (the T^4 dependence is seen only over a short temperature range (figure 5d)). While ρ_0 and ρ_2 for N1a2 are nearly comparable to those obtained for $La_{0.67}(Ca_xSr_{1-x})_{0.33}MnO_3$ films [20], ρ_5 for N1a2 is two orders of magnitude higher, which points to stronger electron–phonon coupling in the oxygen deficient NSMO films.

The absence of the T^2 term in N1a1 points to a connection between bond disorder and magnon scattering. Bond disorder implies spin disorder, which would reduce the magnon density. Thus magnon scattering in the case of N1a1 is probably strong enough only to lower the T^5 dependence. Thus single magnon scattering events gain prominence in the NSMO film only after the second anneal which reduces the oxygen deficiency. While the T^4 temperature dependence for N1a1 may arise due to oxygen deficiencies the exact nature of the scattering mechanism is not clear.

Jaime *et al* [19] used the ratio $\rho_2/\gamma = 1 \times 10^{-5}\ \Omega$ cm (mole K/mJ)^2, where γ is the coefficient of the electronic specific heat, known as the Kadowaki–Woods parameter to argue against electron–electron scattering, having obtained a value 60 times the above value. While ρ_2 for N1a1 is about 3 times greater than that reported by Jaime, γ for NSMO ($x = 0.33$) has been reported to be 25 mJ/mol K^2 [22], much larger than the 4 mJ/mol K^2 (from [23]) used by Jaime. Using $\gamma = 25$ mJ/mol K^2 for N1a2 we obtain a value of $6.3 \times 10^{-5}\Omega$ cm(mole K/mJ)^2. Though this is much closer to the ideal ρ_2/γ it cannot

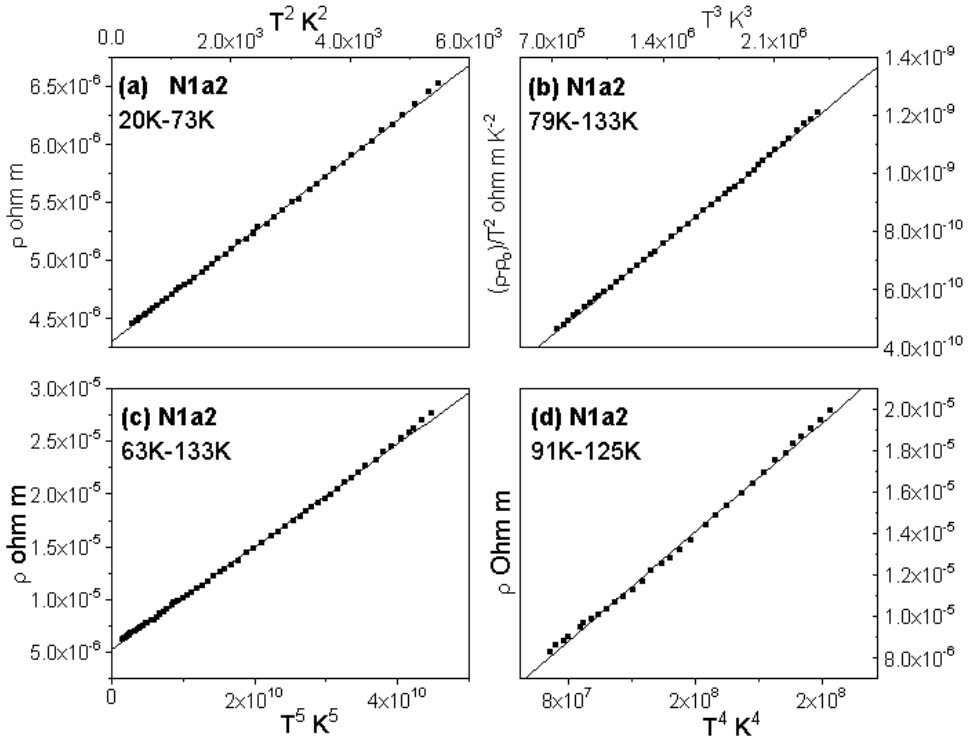

Figure 5. (**a, b**) Fits to eq. (2) for N1a2, (**c, d**) the T^5 and T^4 dependence of $\rho(T)$ for N1a2 respectively.

be used to argue in favour of electron–electron scattering in oxygen deficient samples since the enhancement in γ has been attributed to a coupling between the Nd and Mn spins [22].

With this value of γ for NSMO $(x = 0.33)$ we determine the density of states $N(E_{\rm F})$, the Fermi level $E_{\rm F}$ and the effective mass. We use these parameters along with the value of the spinwave stiffness constant D obtained from inelastic neutron scattering [24] in the following expression for ρ_2 [19] to calculate the electron–magnon coupling energy $NJ\{NJ = W - E_{\rm F}$ (where $2W$ is the e_g bandwidth)$\}$.

$$\rho_2 = \frac{9\pi^3 N^2 J^2 \hbar^5 k_{\rm B}^2}{8e^2 E_{\rm F}^4 k_{\rm F} (m^* D)^2} I(\varepsilon), \tag{3}$$

where $I(\varepsilon) = \int_{\varepsilon}^{\infty} x^2/(\sinh^2 x)\mathrm{d}x$ with $\varepsilon = Dq_{\rm min}^2/2k_{\rm B}T$; $Dq_{\rm min}^2$ is the minimum energy that connects up-spin and down-spin bands. $I(\varepsilon) \approx 1.4$ (between 20 K and 75 K where the T^2 dependence is observed). The above expression is an extension of the standard perturbation calculation of Mannari [26] by Jaime *et al* [19] in which the minority-spin sub-band is shifted in energy such that its Fermi momentum differs by an amount $q_{\rm min}$ from that of the majority sub-band.

Table 4. Parameters calculated from γ, ρ_2 and D for N1a2 as described in the text.

Parameter	$La_{0.67}(Pb, Ca)_{0.33}MnO_3$ Jaime *et al* [19]	N1a2
γ mJ/mol K^2	4*	25 [22]
D meV $Å^2$	140	165† [24]
$N(E_F)$ energy states/eV m^3	1.1×10^{28}	6.4×10^{28}
m^*/m	2.5	8.8
E_F eV	0.5	0.13
$NJ = W - E_F$ eV	1	0.14
Bandwidth (2W) eV	3	0.55

*For LCMO (0.33).
†For NSMO (0.3).

N1a2 has a much smaller bandwidth, and weaker electron–magnon coupling strength compared to Jaime *et al*'s single crystal data (table 4). As a consequence the $\rho_{300\ K}$ for N1a2 is at least an order of magnitude larger than that for the crystal. According to the double exchange interaction [25] the ferromagnetic coupling between the Mn spin cores depends on the angle between the t_{2g} spins and the width of the e_g band which is dependent on the oxygen stoichiometry. The narrow bandwidth results in a lesser T_P (194 K) for N1a2 than that of its bulk target which had a T_P of 241 K.

ρ_5 the coefficient of the T^5 term in eq. (2) was used to determine the Debye temperature (Θ_D) using the expression for ρ_5 in [26]. These resulted in Θ_D values, much lesser than those obtained from specific heat measurements (see for eg. [27]), which shows that conventional electron–phonon coupling cannot be used to describe the observed high temperature T^5 dependence of the resistivity.

3.3 *Thermopower*

The Seebeck coefficient $(S(T))$ provides additional information about the nature of the high temperature transport. $S(T)$ for N1a1 has a prominent peak around 195 K similar to that reported by Jaime *et al* [12] (figure 6a). Above this temperature $S(T)$ has the form [12]

$$S = \frac{k_B}{e}\left[\frac{E_S}{k_B T} - \ln\left(\frac{5}{4}\right) - \ln\left(\frac{c(1-c)}{(1-2c)^2}\right)\right], \tag{4}$$

where E_S is the activation energy and c the polaron concentration. The first term is typical of thermally activated transport. The second term represents the spin entropy of a spin-3/2 hole moving in a spin-2 background and the third term represents mixing entropy in the case of correlated hopping with near neighbour repulsion. Using the intercepts of the S vs $1/T$ plot and eq. (4) we get $E_S = 12.2$ meV and $c = 0.28$ for N1a1. This value of E_S is slightly greater than the 10 meV reported by Jaime *et al* [12]. The large difference between E_A (146.5 meV) and E_S values is the hallmark of polaronic transport. c is much less than

the ideal value of 0.33 again indicative of the oxygen deficiency in the lattice. Using the formula $La^{3+}_{1-x}A^{2+}_{x}Mn^{3+}_{1-x+2y}Mn^{4+}_{x-2y}O^{2-}_{3-y}$ we determine the oxygen deficiency $y = 0.025$ for N1a1. $S(T)$ for N1a2 is negative throughout the range of measurement and a very broad peak is seen around $T_{\rm P}$ (195 K). Above $T_{\rm P}$, $S(T)$ still obeys eq. (4) with $c = 0.32$ ($y = 0.005$ for N1a2) and $E_{\rm S} = 11.4$ meV (figure 6a (inset)). Thus annealing at a higher temperature has resulted in a reduction of $E_{\rm S}$ and an increase in the polaron concentration. An estimate of the carrier concentration can be obtained by setting $n = c/a^3$. This gives $n = 4.8 \times 10^{27}/\mathrm{m}^3$ for N1a1 and $5.5 \times 10^{27}/\mathrm{m}^3$ for N1a2.

As a result of strong electron–phonon coupling, the spin entropy in the manganites gets added to the electron entropy (seen in samples with low dopant concentration or a high defect concentration/oxygen deficiency) resulting in a peak in $S(T)$ due to the ordering of Mn spins across $T_{\rm C}$ as seen for N1a1 and N2a1 and can be related to the peak observed in specific heat [28]. If the electron–phonon coupling is not strong enough, only a change in slope is seen in $S(T)$ typical of a metal–insulator transition. Thus in N1a2 the electron–phonon coupling is weaker and $S(T)$ tends towards a broad slope change as seen in the bulk target (figure 6a).

$S(T)$ for as-prepared film N2 increases rapidly as the temperature is lowered indicative of an excitation to a mobility edge. Upon annealing at 800°C a small peak is seen across $T_{\rm P}$ (figure 6b).

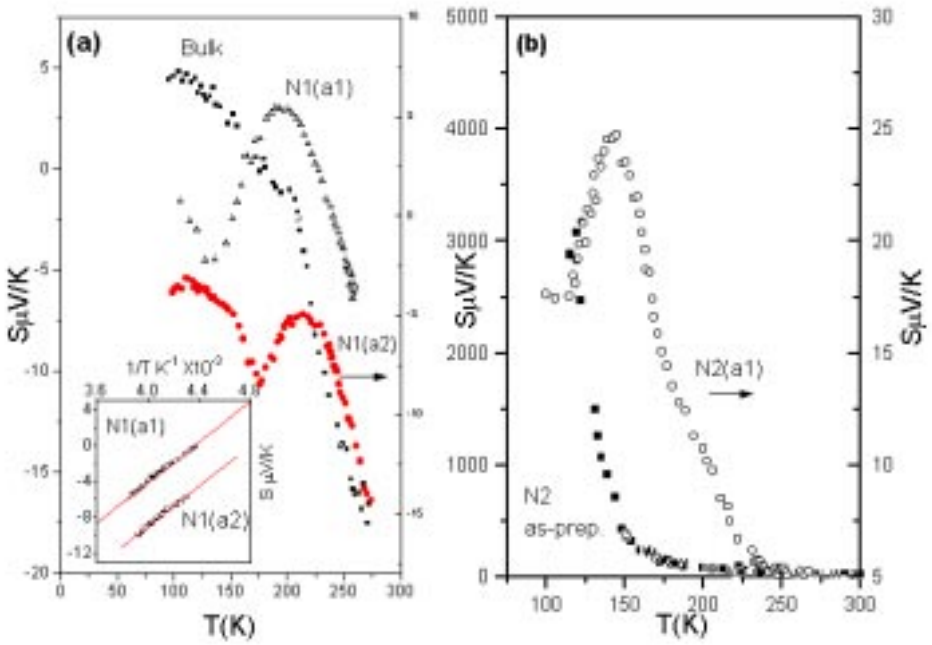

Figure 6. (**a**) $S(T)$ for N1a1, N1a2 and the bulk target. The inset shows the high temperature fits to eq. (4) for N1a1 and N1a2, (**b**) $S(T)$ for as-prepared N2 and N2a1.

3.4 *Magnetoresistance measurements*

It is now widely accepted that the temperature and magnetic field dependence of the CMR manganites can be classified into two categories [29]. In single crystals and epitaxial films very large MR values have been found near $T_{\mathrm{C}}/T_{\mathrm{P}}$ and very small MR values at low temperatures ($< 1\%$ MR for $T \sim 0.1\ T_{\mathrm{C}}$). MR($H$) for single crystals is found to be linear at low temperatures [29]. In polycrystalline bulk and thin films the observed low temperature MR (LTMR) is very high (30–40%) MR for ($T \sim 0.1\ T_{\mathrm{C}}$) [30]. MR($H$) for polycrystalline materials is essentially non-linear with a much sharper response to small field changes (i.e. large low field MR) [29,30].

Magnetoresistance measurements on N1a1 show considerable low temperature MR (38% at 20 K under a 6.4 T field) (figure 7a and table 5) comparable to those seen in polycrystalline samples [30]. However unlike polycrystalline samples MR(H) is seen to be linear at low temperatures. While the large MR observed in polycrystalline samples is due to magnetotunnelling across grain boundaries the effect observed here is due to incomplete magnetization due to oxygen vacancies. Upon annealing at 1000°C there is a large reduction in the MR at 4.2 K, pointing to better homogenization of the lattice.

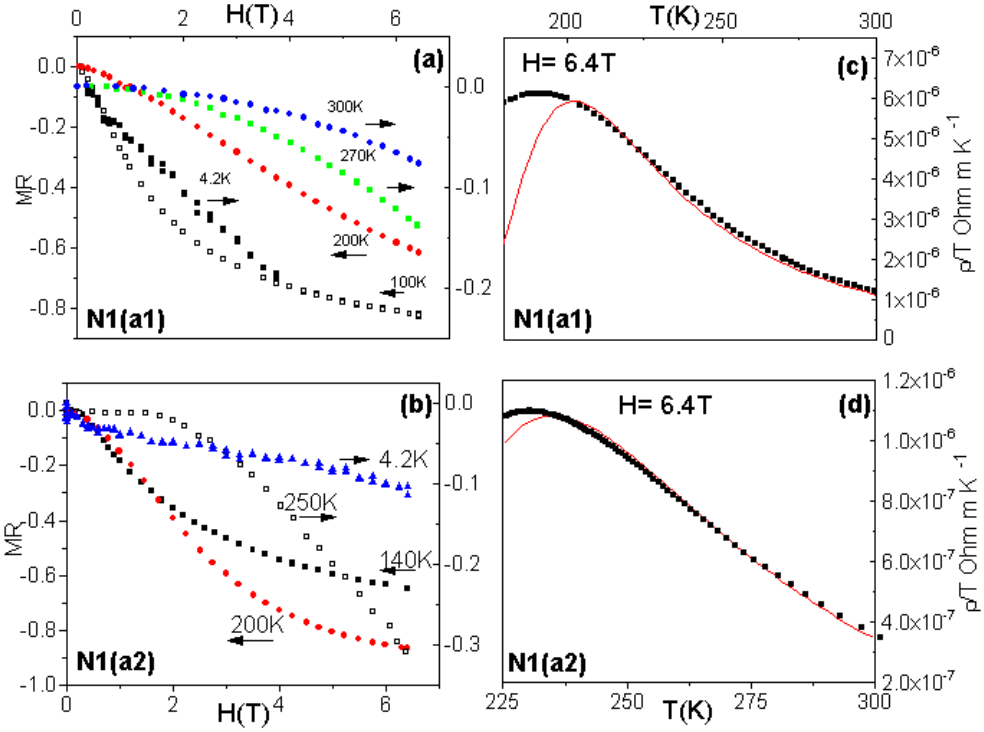

Figure 7. (**a, b**) MR(H) at various temperatures for N1a1 and N1a2 respectively, (**c, d**) fits of $\rho(T, H = 6.4T)$ to eq. (5) for N1a1 and N1a2 respectively.

Table 5. Low temperature magnetoresistance for N1 and the bulk target.

Sample	% MR at 4.2 K ($1T$)	% MR at 4.2 K ($6.4T$)
NB ($T_{\rm P} = 241$ K)	18.3	49.1
N1a1 ($T_{\rm P} = 165$ K)	5.3	30.2
N1a2 ($T_{\rm P} = 196$ K)	3.8	11.4

A T^4 and T^5 dependence of $\rho(T, 6.4T)$ was seen in overlapping temperature ranges with much smaller values of ρ_4 and ρ_5. The large decrease in the ρ_4 due to the external magnetic field could point to a strong magneto-elastic coupling (since phonon processes are expected to contribute to both exponents).

For temperatures just below $T_{\rm P}$, the MR(H) curve has a positive curvature while above $T_{\rm P}$ the curve has a negative curvature (convex with respect to the origin). This behaviour is similar to those seen by Broussard *et al* [20]. MR(H) curves for N1a2 follow similar trends (figure 7b).

Well above $T_{\rm C}$, the existence of magnetic polarons has been reported for manganites [31]. Accordingly, the activation energy has an additional exchange dependent term above $T_{\rm P}$ [13]. The field dependent resistivity for adiabatic hopping transport can be written as

$$\rho(T, H) = \rho_0 T \exp\left[\frac{E_{\rm A}}{k_{\rm B}T}\{1 - B_J(T - T_{\rm C}, H)B_J(N_p, T - T_{\rm C}, H)\}\right]. \quad (5)$$

The exchange contribution is taken into account via a Brillouin function, which represents the interaction between a single spin and a magnetic polaron consisting of a cluster of N_p Mn ions. As a result, the observed MR well above $T_{\rm C}$ exhibits a H^2 dependence [13] which explains the concavity seen in the MR(H) plot above $T_{\rm P}$. Equation (5) was fitted to $\rho(T, H = 6.4T)$ for N1. Data for N1a1 was fitted with $T_{\rm C} = 157.1$ K and $N_p = 3.4$ above $T_{\rm P}$ (=198 K at 6.4T). A $T_{\rm C}$ of 183.6 K and an N_p of 4.4 was obtained for N1a2 (figures 7c, d). Thus the cluster size increases when the disorder decreases.

3.5 *Discussion*

To understand the effect of oxygen vacancies on the transport properties of manganites we begin with the effect of annealing on the lattice constant (a_0). It has been well established that varying the oxygen content in the manganites results in a change of the Mn^{3+}/Mn^{4+} ratio (i.e. the carrier concentration) [3]. Thus progressive annealing reduces the oxygen deficiency which is accompanied by a corresponding decrease in the Mn^{3+}/Mn^{4+} ratio. Since Mn^{4+} is a smaller ion than Mn^{3+} there is a decrease in a_0. From our thermopower data we estimate a Mn^{4+} content of 28% in N1a1 and 32% in N1a2. This increase in carrier concentration brings about a large decrease in the room temperature resistivity and an increase in $T_{\rm P}$. This increase in $T_{\rm P}$ upon annealing can be understood in the following way. According to the double exchange mechanism ferromagnetism in these compounds arises by the indirect coupling of the manganese d-shells via the conducting electrons. Thus the ferromagnetism is conduction electron dependent and the strength of the exchange integral (and hence $T_{\rm C}$/ $T_{\rm P}$) would depend on the carrier concentration. Annealing makes

the lattice more homogenous and as a result the average barrier to the polarons motion in the lattice is reduced as reflected in the decrease in E_{A} [2].

We notice that the resistivity coefficient B in eq. (1a) decreases upon annealing. This could be because of a change in c (the carrier concentration), ν (the longitudinal optical phonon frequency) and a (the hopping distance). Of these the most dramatic change occurs in c as seen from the thermopower measurements. If we assume that $a \sim a_0$ and calculate ν, we see that it almost doubles upon progressive annealing (table 2). Thus an increase in ν which is identified with the hopping frequency or the attempt rate is indicative of lesser localization. Conversely if we use a value of 10^{14} s^{-1} for ν, use c from $S(T)$ data and calculate a the hopping distance or the hopping amplitude we find that we end up with values which are nearly equal to a_0 in both cases. Thus we see that annealing influences the hopping frequency more than the hopping amplitude. Thus more the bond disorder lesser the carrier concentration and more the localization, therefore lesser is the exchange interaction resulting in a lower T_{P}.

The absence of the T^2 dependence in the low temperature resistivity in N1a1 indicates the presence of inhomogenous magnetization well below T_{C}. The close correlation between magnetization and MR in these systems has been well established [29]. A large applied field lines up the spin throughout the lattice resulting in the large observed MR. Upon annealing this film at 1000°C we find that the T^2 dependence is now seen in the low temperature resistivity. However using eqs (2) and (3) we find that N1a2 has a much lower bandwidth and electron–magnon coupling energy than $La_{0.67}(Pb,Ca)_{0.33}MnO_3$ single crystal [19] indicative of the effect of oxygen deficiencies (table 4).

In conclusion we have made a systematic study of the annealing dependence of the lattice constant, magnetoresistance and thermopower in NSMO films and find that progressive annealing results in a large reduction in oxygen deficiency resulting in lower resistivities, lower activation energies, a higher polaron concentration and a larger polaronic cluster above T_{P}. The magnon contribution to the low temperature resistivity is suppressed in a highly oxygen deficient film and gains prominence only after homogenization of the lattice due to annealing. Of the two films studied the CMR properties of N1 (NSMO film on $LaAlO_3$) improved with progressive annealing while N2 (NSMO film on amorphous alumina) became semiconducting upon annealing at 1000°C. This could be due to aluminium diffusing into the film and is a limitation of using these substrates.

References

[1] W Westerburg, F Martin, S Friedrich, M Maier and G Jakob, *J. Appl. Phys.* **86**, 2173 (1999)
I Panagiotopoulos, C Christides, M Pissas and D Niarchos, *Phys. Rev.* **B60**, 485 (1999)

[2] D C Worledge, G Jeffery Snyder, M R Beasley, T H Geballe, Ron Hiskes and Steve DiCarolis, *J. Appl. Phys.* **80**, 5158 (1996)

[3] Kannan M Krishnan and H L Hu, *Phys. Rev.* **B60**, 14793 (1999)

[4] E Gommert, H Cerva, J Wecker and K Samwer, *J. Appl. Phys.* **85**, 5417 (1999)

[5] H D Peng, B R Zhao, Z Xie, Y Lin, B Y Zhu, Z Hao, Y M Ni, H J Tao, X L Dong and B Xu, *Appl. Phys. Lett.* **74**, 1606 (1999)

[6] K H Dahmen and M W Carris, *J. Alloy and Compounds* **251**, 270 (1997)

[7] H L Ju, J Gopalakrishnan, J L Peng, Qi Li, G C Xiong, T Venkatesan and R L Greene, *Phys. Rev.* **B51**, 6143 (1995)

[8] J Holc, D Kuscer, M Hrovat, K S Berni and K Drago, *Solid state ionics, diffusion and reactions* **95**, 259 (1997)

[9] G Jakob, W Westerburg, F Martin and H Adrian, *Phys. Rev.* **B58**, 14966 (1998)
[10] D Emin and T Holstein, *Ann. Phys.* **53**, 439 (1969)
D Emin, *Adv. Phys.* **24**, 305 (1975)
[11] Y Okimoto, T Katsufuji, T Ishikawa, A Urshibara, T Arima and Y Tokura, *Phys. Rev. Lett.* **75**, 109 (1995)
[12] M Jaime, M B Salamon, M Rubinstein, R E Treece, J S Horwitz and D B Chrisey, *Phys. Rev.* **B54**, 11914 (1996)
[13] G Jakob, W Westerburg, F Martin and D H Adrian, *J. Appl. Phys.* **85**, 4803
[14] P Schiffer, A P Ramirez, W Bao and S W Cheong, *Phys. Rev. Lett.* **75**, 3336 (1995)
[15] E S Vlakhov, R A Chakalov, R I Chakalova, K A Nenkov, K Doerr, A Handstein and K H Mueller, *J. Appl. Phys.* **83**, 2152 (1998)
[16] A Urshibara, Y Moritomo, T Arima, A Asamitsu, G Kido and Y Tokura, *Phys. Rev.* **B51**, 14103 (1995)
[17] K Kubo and N Ohata, *J. Phys. Soc. Jpn.* **33**, 21 (1972)
[18] G J Snyder, R Hiskes, S DiCarolis, M R Beasley and T H Geballe, *Phys. Rev.* **B53**, 14434 (1996)
[19] M Jaime, P Lin, M B Salamon and P D Han, *Phys. Rev.* **B58**, R5901 (1998)
[20] P R Broussard, S B Qadri, V M Browning and V C Cestone, *J. Appl. Phys.* **85**, 6563 (1999)
[21] A Tiwari and K P Rajeev, *Solid State Commun.* **111**, 33 (1999)
[22] J E Gordon, R A Fisher, Y X Jia, N E Phillips, S F Reklis, D A Wright and A Zettl, *Phys. Rev.* **B59**, 127 (1999)
[23] J J Hamilton, E L Keatley, H L Ju, A K Raychaudhuri, V N Smolyaninava and R L Greene, *Phys. Rev.* **B54**, 14926 (1996)
[24] J A Fernandez-Baca, P Dai, H Y Hwang, C Kloc and S-W Cheong, *Phys, Rev. Lett.* **80**, 4012 (1998)
[25] P W Anderson and H Hasegawa, *Phys. Rev.* **B100**, 675 (1955)
[26] I Mannari, *Prog. Theor. Phys.* **22**, 335 (1959)
[27] Soo Hyun Park, Yoon-Hee Jeong and Ki-Bong Lee, *Phys. Rev.* **B56**, 67 (1997)
[28] R Mahendiran, S K Tiwary, A K Raychaudhuri, T V Ramakrishnan, R Mahesh, N Rangavittal and C N R Rao, *Phys. Rev.* **B53**, 3348 (1996)
[29] H Y Hwang, S W Cheong, N P Ong and B Batlogg, *Phys. Rev. Lett.* **77**, 2041 (1996)
[30] T Venkatesan, M Rajeswari, Zi-Wen Dong, S B Ogale and R Ramesh, *Philos. Trans. R. Soc. London* **A356**, 1661 (1998)
[31] J M De Teresa, M R Ibarra, P A Algarabel, C Ritter, C Marquina, J Blasco, J Garcia, A del Moral and Z Arnold, *Nature* (*London*) **386**, 256 (1997)